Carbon 124 (2017) 506–514

Contents lists available at ScienceDirect

Carbon

journal homepage: www.elsevier.com/locate/carbon

Synergistically assembled MWCNT/graphene foam with highly efficient microwave absorption in both C and X bands

Honghui Chen [a], Zhiyu Huang [a], Yi Huang [a, *], Yi Zhang [b], Zhen Ge [a], Bin Qin [a], Zunfeng Liu [c], Qian Shi [a], Peishuang Xiao [a], Yang Yang [a], Tengfei Zhang [a], Yongsheng Chen [a]

[a] Tianjin Key Laboratory of Metal and Molecule Based Material Chemistry, Key Laboratory of Functional Polymer Materials, State Key Laboratory and Institute of Elemento-Organic Chemistry, Collaborative Innovation Center of Chemical Science and Engineering (Tianjin), National Institute for Advanced Materials, School of Materials Science and Engineering, Nankai University, Tianjin 300071, China

[b] Beijing Institute of Aeronautical Materials, Beijing 100095, China

[c] State Key Laboratory of Medicinal Chemical Biology, College of Pharmacy, Nankai University, Tianjin 300350, China

A R T I C L E I N F O

Article history:
Received 23 July 2017
Received in revised form
24 August 2017
Accepted 2 September 2017
Available online 5 September 2017

A B S T R A C T

It is a great challenge to fabricate lightweight microwave absorption materials (MAMs) with strong electromagnetic wave attenuation over wide frequency range. In this work, ultralight multiwalled carbon nanotube (MWCNT)/graphene foams (CGFs) are prepared through a facile solvothermal method and their microwave absorption (MA) properties are fully investigated. The CGFs exhibit tunable complex permittivity and conductivity through regulating MWCNT loading and thermal reduction temperature. The addition of MWCNT remarkably enhances the MA intensity of CGFs in low frequency. A minimum reflection loss value of −39.5 dB and average absorption intensity exceeding 22.5 dB in both C (4–8 GHz) and X (8–12 GHz) bands are obtained. For the optimized CGF, the qualified bandwidth with reflection loss less than - 10 dB reaches up to 16 GHz, which covers the whole measured range of 2–18 GHz and shares the widest qualified bandwidth among open literature reports. Furthermore, a specific MA performance of 12243 dB cm^2 g^{-1} is realized, which is one of the best results among various MAMs. The synergistic effect of MWCNT and graphene and thus obtained three dimensional high loss multilevel network architecture are thought to be the primary causes for the excellent MA performance of CGFs.

1. Introduction

With the explosive development of information technology, high-performance broadband and lightweight microwave absorption materials (MAMs) have drawn increasing attentions due to the important role they played in human health, information safety, military stealth and elimination of electromagnetic interference (EMI) caused by communication and navigation systems [1–4]. Generally, interfacial impedance matching and electromagnetic wave losing are considered as the two primary factors in affecting the microwave absorption (MA) properties of materials [5,6]. Over the past few decades, to achieve MAMs with strong MA intensity and wide absorption bandwidth, tremendous efforts have been made to optimize the physicochemical properties of MAMs for obtaining desired permittivity and permeability, which fundamentally effect the interfacial impedance gap and electromagnetic wave attenuation ability [7–10]. Considerable progress has been made in designing MAMs with hierarchical structure, such as yolk–shell CoNi@Air@TiO_2 and dendrite-like γ-Fe_2O_3 [2,11], to broaden absorption bandwidth. Besides, heat-resistant and frequency-tunable MAMs have also been studied extensively [3,9,12–15]. Nevertheless, MAMs exhibiting comprehensive advantages of strong absorption, wide absorption bandwidth, and low density are quite limited. In addition, most reported MAMs just exhibit one absorption peak in specific frequency range, mainly in X band (8–12 GHz) or Ku band (12–18 GHz). Achieving MAMs with multiple absorption peaks and strong MA performance in both C and X bands remains a huge challenge.

Nanocomposites based on three dimensional (3D) graphene materials have caught wide attention for their potential in electromagnetic wave attenuation [16–18]. Benefiting from the

* Corresponding author.
E-mail address: yihuang@nankai.edu.cn (Y. Huang).

http://dx.doi.org/10.1016/j.carbon.2017.09.007
0008-6223/

excellent physicochemical properties originated from graphene sheet and distinctive structure, 3D graphene materials have shown various potential applications, such as environmental remediation, catalysis, photo-thermal conversion and energy storage [19–21]. Recently, we have demonstrated the broadband absorption of graphene foam (GF) with 3D interconnected network [22], which was distinct from the very narrow absorption bandwidth that using graphene just as a filer [23,24]. Nevertheless, restricted by the intrinsic electromagnetic properties of graphene, the MA property of GF in low frequency (e.g. C band (4–8 GHz)), is usually unsatisfactory [5]. As the building block of 3D GF, the large graphene sheets are ideal carrier for loading various nanomaterials, such as magnetic nanoparticles and carbon nanotubes [25–29]. Therefore, we have been trying to develop multicomponent macroscopic 3D composite foam to take the full advantages of all components to enhance the electromagnetic wave attenuation efficiency. Furthermore, it is also possible to regulate the electromagnetic properties of this composite foam by controlling the loading of the guest materials and achieve the synergistic effect of graphene and the filler, which may be able to improve the absorption intensity in both C and X bands.

Carbon nanotubes (CNTs) are widely used as microwave absorber for their remarkable electronic and mechanical properties [30–32]. The unique one dimensional (1D) tubular nanostructure offers enormous sites for electromagnetic wave scattering. Besides, the induced current generated by CNTs under alternating electromagnetic field and enhanced interface polarization also contribute to electromagnetic wave attenuation [33]. However, CNTs are generally served as MA filler and incorporated into polymers. The aggregation and inappropriate processing of CNTs make them hard to form effective attenuation networks in matrix, thus hamper the MA performance [4,34,35]. More recently, 3D CNTs and their composite have shown encouraging progress in EMI shielding application [36,37]. It is thought that building a composite network by integrating 1D CNTs into 3D graphene framework might to be an appropriate route to obtain broadband and high-performance MAMs.

In this work, ultralight multiwalled carbon nanotube (MWCNT)/graphene hybrid foams (CGFs) were prepared using a facile solvothermal self-assembly method, and their outstanding MA performance was demonstrated. The effective absorption bandwidth with reflection loss (RL) less than - 10 dB covers the entire tested frequency range of 2–18 GHz and a minimum RL value of −39.5 dB was realized. Moreover, the introduction of MWCNT observably improved the electromagnetic wave attenuation ability of CGFs in low frequency. The optimized CGFs exhibit two strong absorption peaks and average absorption intensity exceeding 22.5 dB in both C (4–8 GHz) and X bands (8–12 GHz). Our results also indicate that annealing temperature and the mass ratio of graphene/MWCNT have an important influence on the electromagnetic properties. Moreover, the possible MA mechanisms are also explored.

2. Experimental section

2.1. Materials

Graphene oxide (GO), with the lateral dimension mainly above 10 μm, was synthesized from nature flake graphite using a modified Hummers method, as previously reported by our group [38]. The MWCNT (purity >97 wt%, outer diameter 20–40 nm, and length 5–15 μm) supplied by Shenzhen nanotech Port Co., Ltd. (Shenzhen, China). All the other chemicals were purchased from Tianjin Chemical Reagent Co., Ltd. (Tianjin, China) and used as received.

2.2. Preparation of modified MWCNT

For the purpose of removing impurities of raw MWCNT and modifying oxygen functional groups on MWCNT, 1 g raw MWCNT and 100 ml solution of 8 M HNO_3/H_2SO_4 (1/3, v/v) were added in a 250 ml flask, and then the mixture was sonicated for 1 h. The suspension containing MWCNT was then refluxed at 140 °C for 12 h. After cooling down to room temperature, the slurry was filtrated and washed with deionized water until the PH of filtrate reached 7. Then the filtered product was dispersed in water under ultrasonication and then freeze-dried. Finally, the fluffy modified MWCNT powder was obtained (Fig. S1).

2.3. Preparation of ultralight CGFs, C@GFs and C/GFs

Typically, to fabricate CG7F, a certain amount of modified MWCNT was re-dispersed in ethanol. Then the MWCNT/ethanol solution was added into GO ethanol solution (157 ml, 2.0 mg/ml) with the mass ratio of modified MWCNT/GO = 1:7. After mechanical agitation for 2 h, the resultant 628 ml GO/MWCNT ethanol solution (the concentration of GO was 0.5 mg/ml) was solvothermally reacted at 180 °C for 12 h in a home-made Teflon-lined autoclave. After gradually solvent exchange with water and freeze drying, an ultralight foam (CG7F) was obtained. The CG7F-200, CG7F-400, CG7F-500, CG7F-600 and CG7F-800 were finally obtained through annealing the resultant CG7F at 200, 400, 500, 600 and 800 °C for 1 h in argon atmosphere, respectively. Similarly, the CG2F, CG3F, CG5F and CG9F were prepared by the same solvothermal method (the final concentration of GO in GO/MWCNT ethanol dispersion was maintained at 0.5 mg/ml) with the mass ratio of MWCNT/GO = 1:2, 1:3, 1:5, 1:9, respectively. For convenience, the CGFs with the reduction temperature of 200 °C, 400 °C, 500 °C, 600 °C, 800 °C are labeled as CGF-200, CGF-400, CGF-500, CGF-600 and CGF-800, respectively. Besides, neat graphene foams (GFs) without modified MWCNT were also fabricated from 0.5 mg/ml GO ethanol solution in the same way as above.

C@GFs were prepared through freeze drying of the modified MWCNT/GO aqueous solution directly. The concentration of GO in GO/MWCNT ethanol solution was also maintained at 0.5 mg/ml. C@G3F and C@G7F were fabricated with the mass ratio of modified MWCNT/GO = 1:3 and 1:7, respectively. The remaining processes for preparing C@GFs were the same as CGFs.

Modified MWCNT was replaced by raw MWCNT to fabricate raw MWCNT/graphene foams (C/GFs), and the remaining processes for preparing C/GFs were the same as CGFs.

2.4. Characterizations

Scanning electron microscopy (SEM) images were obtained on a LEO 1530 V P field emission scanning electron microscope with 5.0 kV accelerating voltage. Structure information of the samples was examined with X-ray diffraction (XRD) carried out on a Rigaku D/Max-2500 diffractometer with Cu Kα radiation. The Raman spectrum of the samples was investigated on a Renishaw inVia Raman spectrometer using laser excitation at 514.5 nm. The chemical composition of the samples was obtained by X-ray Photoelectron Spectroscopy (XPS) using PHI 5000 VersaProbe (ULVAC-PHI, Japan). Transmission electron microscopy (TEM) was conducted in a JEOL TEM-2100 electron microscope using an acceleration voltage of 200 kV. All the samples were dried in vacuum at 120 °C for 12 h and then their Fourier transform infrared (FT-IR) spectra were analyzed using a FT-IR Spectrometer (Tensor 27, BRUKER).

2.5. MA measurement

The microwave absorbing property was examined with Agilent PNA-X vector network analyzer (N5244A, 10 MHz-43.5 GHz) by measuring the RL value using arch method in the frequency range of 2–18 GHz. To be briefly, four CGFs cut into 90 mm × 90 mm × 10 mm were arranged into a cubic container with internal dimensions of 180 mm × 180 mm × 10 mm. Then the sample was placed on a standard aluminum plate, which has a thickness of 5 mm and high conductivity (no less than 1.0×10^7 S/m), to reflect all the incident microwaves back to the receiving antenna. The measurements were performed at room temperature.

2.6. Electromagnetic parameter measurement

Complex permittivity and permeability of the samples were measured using coaxial-line method on Agilent HP8722ES vector network analyzer in the frequency range of 2–18 GHz. In a nutshell, the nubby foam sample was fully soaked in liquid wax at 80 °C with the auxiliary of vacuum, after cooling down to room temperature, the sample was sanded to the thickness of 2 mm. Finally, a cylindrical-shaped standard test sample (Φ_{out} = 7.00 mm, Φ_{in} = 3.04 mm) was obtained through cutting the 2 mm thickness block with an annular tool.

3. Results and discussion

3.1. CGFs preparation and characterization

As illustrated in Fig. 1, the ultralight CGFs were obtained through scalable self-assembly of MWCNT and GO followed by different annealing process (for more details, please see Experimental Section). The as-prepared cake-like CGFs show high porosity (>99%) and ultralow bulk density (1.32–2.83 mg/cm^3) (Fig. S2). MWCNT was pre-treated with mixed acid to prevent MWCNT bundling and get better interaction with GO. The XPS spectrum of modified MWCNT are shown in Fig. 2a and Fig. S3. The appearance of C–O and C=O peak of the modified MWCNT with calculated oxygen content of 12.8 wt% indicates that MWCNT was successfully functionalized with oxygen functional groups, such as hydroxyl and carboxyl [39]. It is also confirmed by the FT-IR spectrum (Fig. S4) and Raman spectrum, which shown obviously enhanced I_D/I_G value (Fig. S5). The modified oxygen functional groups contribute to preventing the aggregation of MWCNT and making MWCNT disperse more effectively in GO solution. Moreover, the modified MWCNTs and GO sheets act as spacer and anchor site, respectively, and prevent the restacking of graphene s during the self-assembly process.

To comprehend the impact of MWCNT on the microstructure of CGFs, we carried out XRD characterization of various CGFs annealed at 400 °C. Different from the sharp (002) peak of nature flake graphite and the (001) diffraction peak of GO at 11° (Fig. S6), all the CGFs exhibit a very weak broad peak around 23.1° and an additional peak at 26.5°, as can be seen in Fig. 2b. The broad peak around 23.1°, corresponding the (002) plane of reduced GO (rGO), indicates weak long-range re-stacking of graphene sheets [38]. The emerged peak at 26.5° is associated with MWCNT (Fig. S6), as the amount of MWCNT increases, this peak becomes stronger (Fig. 2b). Besides, further raising the annealing temperature of the corresponding CGF, the peak intensity at 26.5° almost keeps constant (Fig. S7). To some extent, these results confirm the function of MWCNT for preventing the re-stacking of graphene sheets.

The Raman spectra of CGFs annealed at 400 °C are shown in Fig. 2c. The I_D/I_G value of a carbon material is associated with the recovery degree of sp^2 carbon structure [40]. With increasing the content of the MWCNT, the 2D peak of CGF-400 increases remarkably (Fig. 2c), and the I_D/I_G ratio decreases notably from 1.55 to 1.16. Meanwhile, compared with GF-400, the CGFs with the same annealing temperature show higher I_D/I_G and lower I_{2D}/I_G (Table S1). As for CG7F, there are obvious reduction of I_D/I_G ratio from 1.61 to 1.47 and enhancement of I_{2D}/I_G ratio from 0.38 to 0.53 with elevated annealing temperature from 200 °C to 800 °C, as shown in Table S1. These results demonstrate that higher annealing temperature contributes to obtaining lower defect level and better graphitization degree of CGF.

The dependence of electrical conductivity of CGF on MWCNT loading and annealing temperature is presented in Fig. 2d. Electrical conductivity is a critical parameter in designing carbon materials for MA application. In contrast to GF, the CGFs exhibit obviously enhanced electrical conductivity (Fig. 2d). With the raise of MWCNT loading, the electrical conductivity values gradually increase. Meanwhile, the electrical conductivity of CGFs shows obviously positive correlation with annealing temperature. These results are in accord with the analysis of Raman results of CGFs (Table S1). That is, the adjustment of MWCNT loading and annealing temperature of a CGF will vary its defect level and graphitization degree at microscopic scale and thus changing its macroscopic electrical conductivity. Moreover, the regulation of pre-loading of MWCNT and post-process annealing temperature will be convenient and accurate in tuning the electromagnetic properties of CGF.

To better understand the morphology of the CGFs and the distribution of MWCNT, we took the cross-sectional SEM photos of CGFs. Compared with GF (Fig. 3d), which show random lap of

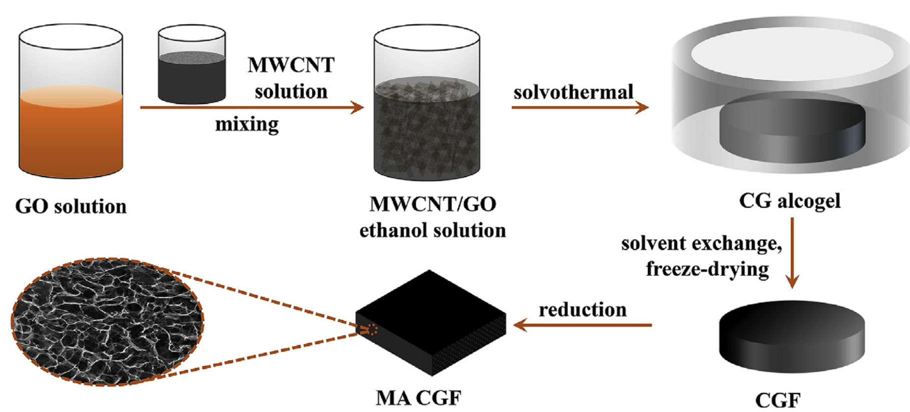

Fig. 1. Schematic illustration of the fabrication process of MA CGF. (A colour version of this figure can be viewed online.)

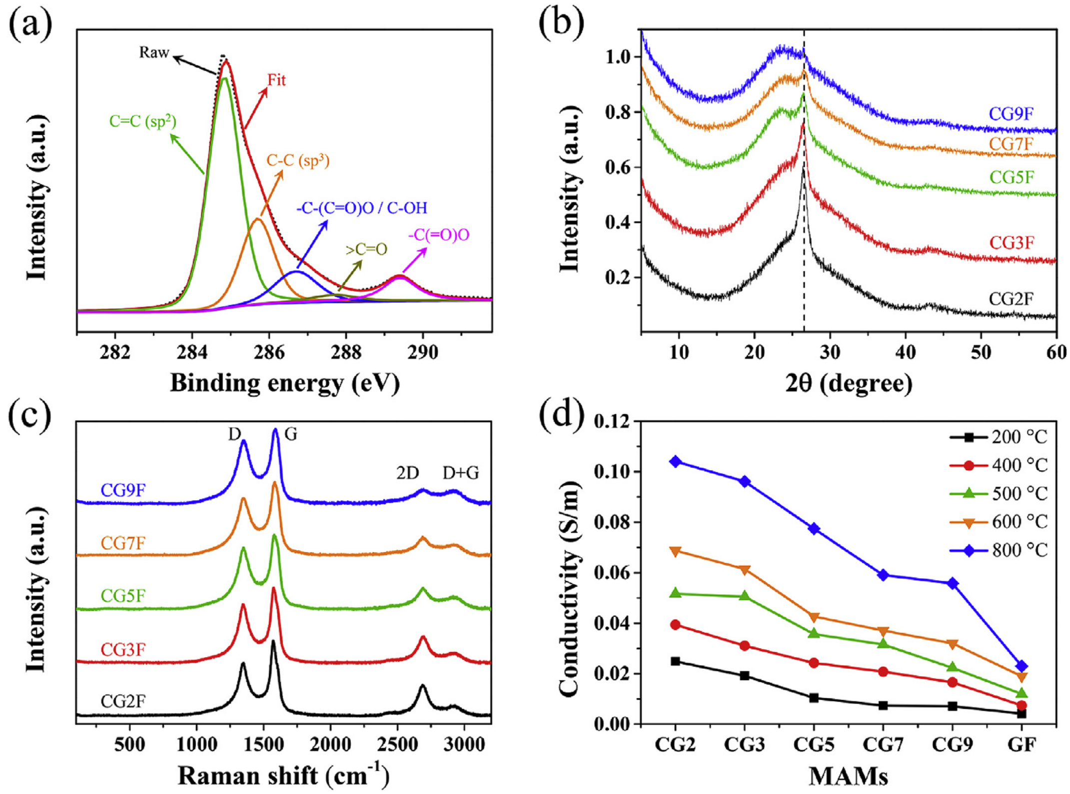

Fig. 2. (a) The XPS spectrum of C1s peaks of modified MWCNT. (b) The XRD spectra of CGFs annealed at 400 °C. (c) The Raman spectra of CGFs annealed at 400 °C. (d) Bulk electrical conductivities versus MWCNT loading for CGFs vary in annealing temperature. (A colour version of this figure can be viewed online.)

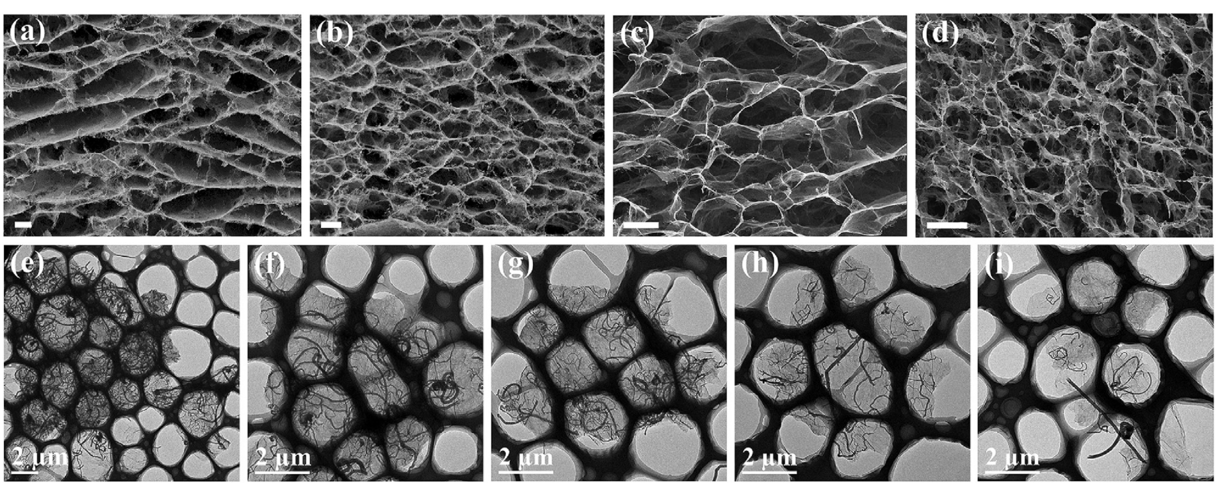

Fig. 3. (a–d) Cross-sectional SEM images of (a) CG2F, (b) CG3F, (c) CG7F and (d) GF. Scale bar, 100 μm (a–d). (e–i) The TEM images of (e) CG2F, (f) CG3F, (g) CG5F, (h) CG7F and (i) CG9F.

graphene sheets and reticulum-like open cell structure with average pore size less than 100 μm, the CGFs possess bigger pore size, more regular and complete pore wall structure (Fig. 3a–c). This can be explained by the reinforcement effect of CNTs [41]. This reinforcement effect would make the in-plane strength of graphene sheets stronger. Moreover, the CGFs exhibit tighter connection among neighboring pore walls, this verifies their elevated electrical conductivity. Besides, it can be seen that the framework of CGF presents gradually distinct anisotropic characteristics as the MWCNT loading increases, the orientation of pore may enhance the response of CGF to electromagnetic wave, as discussed in previous report [36]. The intricately distributed MWCNTs make the surface of the pore wall more rough (Fig. 3a–c compared to Fig. 3d), which is beneficial for electromagnetic wave scattering. The enlarged SEM images of CGFs in Figs. S8 and S9 clearly show the cross-linked structure of graphene sheets and the even-distributed MWCNTs. The MWCNTs which distribute on the edge of graphene sheet can be considered as the scaffold for better connection among the contacted graphene sheets (Fig. S10).

The TEM images of CGFs exhibit the distribution status of

MWCNTs on graphene sheet (Fig. 3 e–i). It can be seen that the surface of graphene sheet in CG2F is full of MWCNTs with various orientation (Fig. 3e). Moreover, randomly oriented MWCNTs are connected to each other so that a complicated interconnected MWCNT network has formed on the graphene sheet. Compared with the CG2F, the CG3F and CG5F show rare MWCNT network because of lower MWCNT loading (Fig. 3f and g). The further reduced MWCNT content makes the MWCNTs in CG7F form a half connected network (Fig. 3h). As for the CG9F, the graphene sheet is scattered with sparse MWCNTs, and almost no MWCNT network has formed (Fig. 3i). These features can be valuable in viewing the role MWCNT network played in the attenuation of electromagnetic waves in CGFs.

3.2. Microwave absorbing properties

The arch method was used to measure the RL values of CGFs in 2–18 GHz (Fig. S11) [22]. Compared with the calculated RL results according to measured electromagnetic parameters, this experimental method, which takes into consideration the matrix and dispersion state of absorber, reflects more reliably the actual MA properties of MAMs [42]. The absorption bandwidth with the RL values lower than −10 dB (more than 90% absorption for incident electromagnetic wave) is widely recognized as the qualified bandwidth [35,43]. (RL is defined as the logarithmic ratio of the reflected wave power of MAM sample plate to the incident wave power and is expressed in dB). Fig. 4 demonstrates the RL curves of CGFs comprehensively in the measured frequency range of 2–18 GHz. It can be found that the minimum RL values of CG2F-200 and CG3F-200 are −32.2 dB at 4.64 GHz and −28.9 dB at 4.96 GHz, respectively, as shown in Fig. 4a. The qualified bandwidths of 2.6–18 GHz for CG2-200 and 2.7–18 GHz for CG3-200 are achieved, which cover C band (4–8 GHz), X band (8–12 GHz), Ku band (12–18 GHz), and also most area of S band (2–4 GHz) [44]. With the decrease of MWCNT loading, the absorbing peak which located in C band becomes weaker and the overall MA performance gets worse. Meanwhile, the GF-200 exhibits one negligible absorbing peak with the minimum RL value of −7.6 dB. These demonstrate that the addition of MWCNT greatly enhances the MA properties of GF in low frequency (especially in C band) and dramatically broadens the qualified bandwidth of CGF.

It is well known that the annealing process is vital to regulate the dielectric properties and electric conductivity of reduced GO, and thus affects the MA properties of the material assembled by reduced GO [5,45,46]. As the annealing temperature increases to 400 °C, the MA performance of CGFs becomes complex (Fig. 4b). In contrast to the RL results of CG2F-200 and CG3F-200, the CG2F-400 and CG3F-400 both show worse MA abilities in low frequency and narrower qualified bandwidth. On the contrary, CG5-400 and CG7-400 exhibit remarkably enhanced MA performance in low frequency. Besides, broader absorption bandwidths are obtained for CG9F-400 and GF-400 compared with CG9-200 and GF-200. The diversiform changing trend of the RL curves of CGFs may ascribe to the increased complex permittivity and electric conductivity caused by thermal annealing, as discussed later. It is notable that a minimum RL value of −39.5 dB at 11.6 GHz is obtained for CG7F-400. Meanwhile, the qualified bandwidth reaches up to 16 GHz, which covers the whole measured range of 2–18 GHz and shares the widest qualified bandwidth in 2–18 GHz among open literature reports. Fig. 4c, d and Fig. S12 show the RL values of CGFs, which are annealed at 500 °C, 600 °C and 800 °C, respectively. It can be seen that the minimum RL value of CGFs obviously shifts to higher frequency and the qualified bandwidth in 2–18 GHz becomes narrower with increased annealing temperature. Moreover, the absorption in low frequency is getting worse. Growing interfacial impedance gap may cause intense surface reflection for

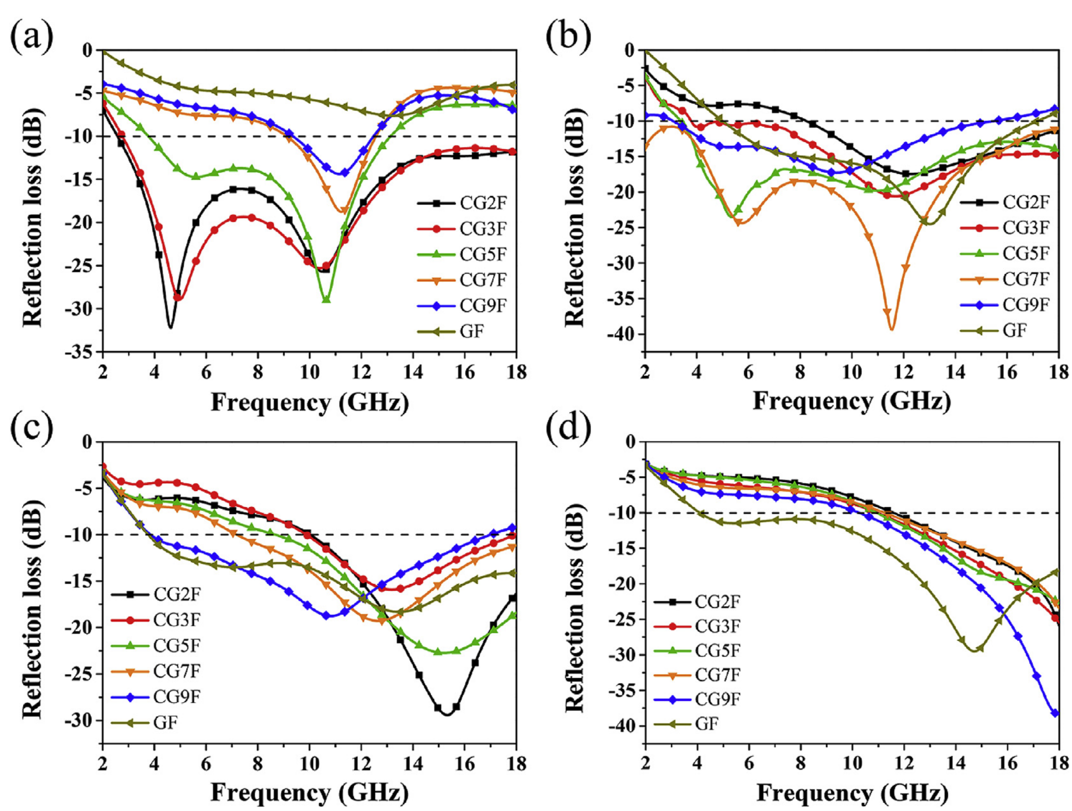

Fig. 4. The RL curves of (a) CGFs-200, (b) CGFs-400, (c) CGFs-500, (d) CGFs-600. (A colour version of this figure can be viewed online.)

electromagnetic wave [47]. This result indicates that excessive thermal reduction of CGFs could be counter-productive and there exists a balance between thermal annealing temperature and MWCNT content for achieving excellent MA performance.

To understand the effect of 3D cross-linked graphene network on the MA properties, the dependence of RL value on the tested frequency, with (CGFs) and without (C@GFs) solvothermal process was investigated (Fig. 5a). C@GFs were obtained through freeze-drying of MWCNT/GO aqueous solution directly followed by annealing process. Obviously, the MA performance is greatly improved by introducing solvothermal procedure (CGFs). The qualified absorption bandwidth of C@GFs is much narrower than that of CGFs. Besides, the absorption of C@GFs in low frequency is weaker. Different from closely cross-linked morphology of CGFs (Fig. 3a–c), C@GFs show loosely lapped structure of graphene sheets (Fig. S13), which results in lower electrical conductivity. For example, the C@G7F-400 shows a conductivity of 5.2×10^{-3} S/m, which is much lower than that of CG7F-400 (2.1×10^{-2} S/m). The difference in morphology and conductivity is evidence that the formed 3D cross-linked graphene structure strengthened by MWCNT network significantly enhances the electromagnetic wave absorption ability of the CGFs.

The disperse state of MWCNT in graphene framework also influenced the MA properties (Fig. S14). The C/GFs, which were fabricated by replacing modified MWCNT with raw MWCNT (without pre-treatment with mixed acid), exhibit thoroughly mediocre MA performance (Fig. S14). This probably because of the poor MWCNT network caused by MWCNT bundling and the very weak connection between MWCNTs and graphene sheets.

As shown in Fig. 5b, all the optimized and representative RL curves of CGFs with various MWCNT contents are illustrated. The optimized CGFs exhibit wide qualified bandwidth in 2–18 GHz and strong absorption in C band and X band. Besides, the MA ability in S band also gets enhanced to some extent. Obviously, excellent MA performance of CGFs with low annealing temperature, such as CG2F-200 and CG3F-200 (annealed at 200 °C), could be achieved with high MWCNT loading. On the other hand, the CGFs with low MWCNT loading need to be annealed at higher temperature to obtain better MA performance, e.g. CG7-400 (annealed at 400 °C). So MWCNT plays a vital role in improving the MA performance of CGFs, especially in low frequency.

A comprehensive literature review of previous reported MAMs clearly indicates the superiority of our CGFs serving as high-performance MAMs (Table S2). The CGFs possess the advantage of broad qualified bandwidth and very high average absorption intensity (defined as *AAI*, high *AAI* value means strong absorption of a MAM in the whole measured frequency range. For more details, please see Supporting Information) (Fig. 5c). The CG7F-400 exhibits best *AAI* (19.1 dB) among all the previous reported MAMs in 2–18 GHz. Besides, The CG7F-400 and CG3F-200 show an average *AAI* exceeding 22.5 dB in the whole 4–12 GHz (Table S2) and dominant absorption in C band (Fig. S15). In contrast, the carbon foam merely owns a *AAI* of 9.5 dB in 2–18 GHz [48].

Density and thickness are highly valuable factors need to be considered for microelectronic devices and aerospace applications in addition to qualified bandwidth and *AAI* [5], so we introduced a more realistic parameter of specific MA performance (*SMAP*) which is defined as the ratio of *AAI* to the product of density and thickness

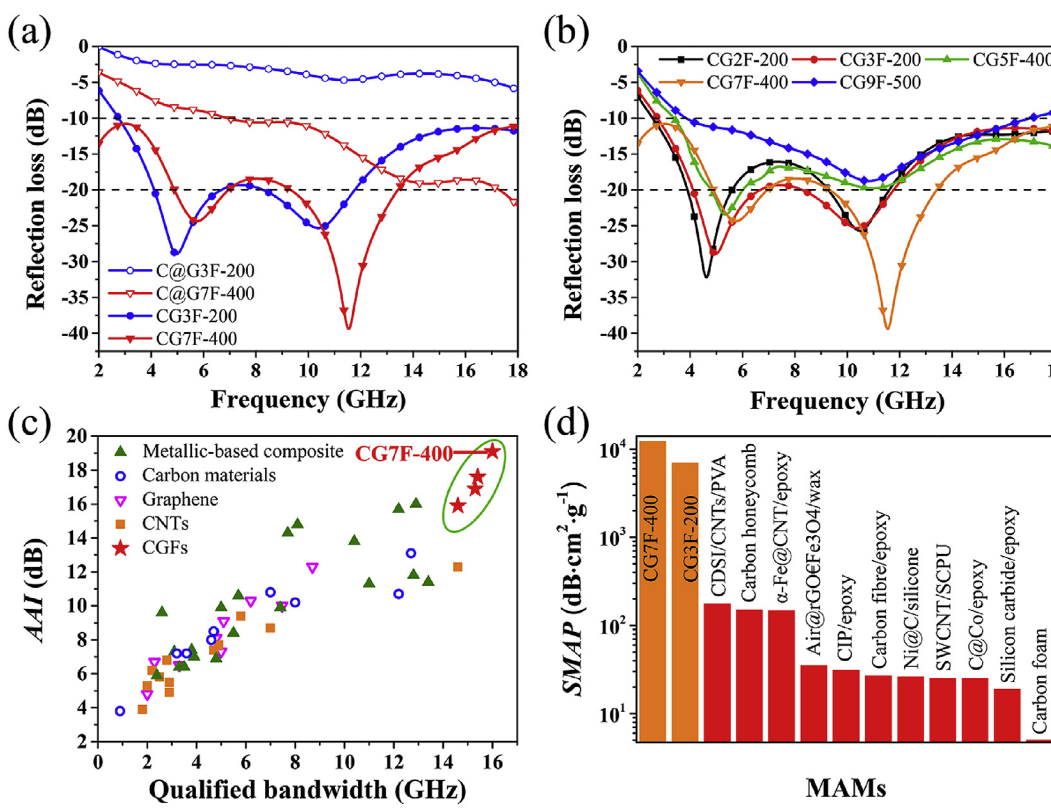

Fig. 5. (a) Frequency dependence of RL values of C@GFs and CGFs. (b) The representative RL curves of CGFs with different MWCNT content at optimized annealing temperature. (c) *AAI* versus qualified bandwidth of different MAMs in 2–18 GHz. Each symbol indicates a kind of material category as follows: metallic-based composite (magenta filled up triangle), carbon materials (blue filled circle), graphene-based materials (black filled down triangle), CNTs (orange filled square), CGFs (red star). A detailed description of each data point is presented in Table S2. (d) *SMAP* values comparison of the representative MAMs in 2–18 GHz. The *SMAP* data of more MAMs is listed in Table S2. (A colour version of this figure can be viewed online.)

($AAI/(d \cdot t)$). The *SMAP* for CGFs are much higher than other kinds of MAMs (Table S3). As optimum CGFs, the CG7F-400 shows a *SMAP* of 12243 dB cm^2 g^{-1}, which is well above the known MA composites (not exceeding 200 dB cm^2 g^{-1}), such as carbon powder coated honeycomb (~150 dB cm^2 g^{-1}) and silicon carbide/epoxy composite (~19 dB cm^2 g^{-1}) (Fig. 5d). It is worth noticing that the CG7F-400 holds the widest qualified bandwidth (16 GHz), the highest *AAI* (19.1 dB) and *SMAP* in the range of 2–18 GHz and has the best *AAI* (22.7 dB) in 4–12 GHz, these results are superior to all the available MA materials have been reported before.

3.3. Electromagnetic properties and mechanism

It is well known that the relative permittivity (ε) and permeability of a MAM greatly influence its MA performance [49,50]. Therefore, to explore the possible MA mechanism of the CGFs, we measured the electromagnetic parameters of the CGFs. Fig. 6 shows the frequency dependence of real part of permittivity (ε') and dielectric loss tangent ($\tan \delta_e$) of CGFs-200 and CGFs-400. Obviously, either the increase of MWCNT content or elevating annealing temperature can lead to the increment of ε' (Fig. 6a and c). For typical dielectric MAMs, the relaxation loss originated from polarization processes and conductance loss due to the moving of charge carriers under applied electromagnetic field dominantly contribute to the increase of imaginary part of permittivity (ε'') [51]. Owing to the formed interlaced network of MWCNT, the CGFs show higher bulk electrical conductivity (Fig. 2d) and polarization loss. Meanwhile, the elevated annealing temperature also facilitates the increase of conductance loss. Therefore, the ε'' also exhibits positive correlation with the MWCNT content and annealing temperature (Fig. S16). The $\tan \delta_e$ ($=\varepsilon''/\varepsilon'$) represents the capability of dissipating microwave energy [2,52]. Compared with the $\tan \delta_e$ of CGFs-200, the CGFs-400 show more complex $\tan \delta_e$ (Fig. 6b and d), especially in low frequency range, this may result from the comprehensive effect caused by MWCNT content and annealing temperature, and thus lead to the complex MA results in low frequency. Therefore, to achieve better MA performance, a trade-off between permittivity and dielectric loss is necessary to balance the impedance matching and electromagnetic wave attenuation [53]. Based on this, we ascribe the excellent MA performance of the optimized CGFs to the following three aspects:

Firstly, well-balanced dielectric properties originated from appropriate MWCNT content and annealing temperature. According to the frequency dependence of complex permittivity and dielectric loss tangent (Fig. 6 and Fig. S15), both the ε' and ε'' show positive correlation with either MWCNT content or annealing temperature. Therefore, through regulating the MWCNT content and annealing temperature, the optimized CGFs can be endowed with proper ε and electric conductivity, thus achieving balance between impedance matching and electromagnetic wave attenuation.

Secondly, distinctive multilevel structure for multiple scale scattering and polarization attenuation. The ultrahigh porosity and relative low ε' of the optimized CGFs ensure that most incident microwaves are able to penetrate into the inside of porous CGFs. The enormous MWCNTs and graphene domains which distribute on the pore walls scatter the propagated electromagnetic wave repeatedly (Fig. 7a). Besides, massive positive and negative charged domains are formed on the pore wall under alternating electromagnetic field, leading to responsive polarization losses, which in turn improve the overall absorption.

Lastly, giant 3D cross-linked and intricate loss network stemming from the synergistic effect of 1D MWCNT and 2D graphene. Benefiting from the high aspect ratio and large sheet size of GO, the

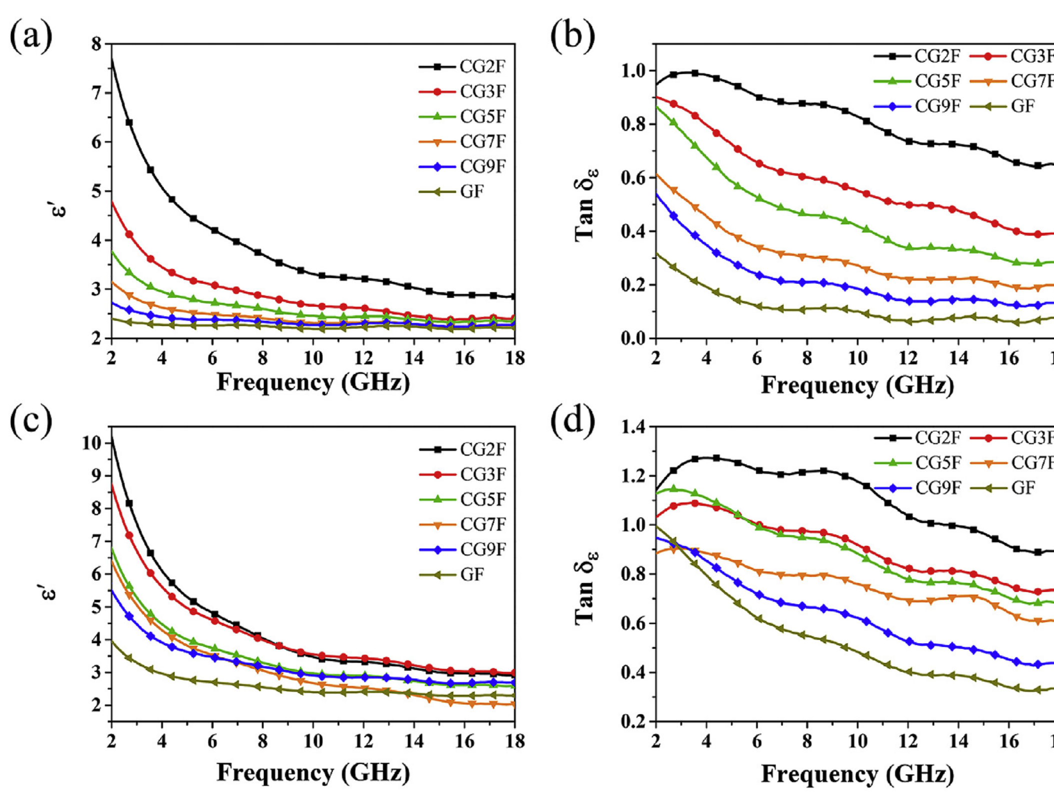

Fig. 6. (a) Real parts of complex permittivity and (b) dielectric loss of CGFs-200 in the frequency range of 2–18 GHz. (c) Real parts of complex permittivity and (d) dielectric loss of CGFs-400 in the frequency range of 2–18 GHz. (A colour version of this figure can be viewed online.)

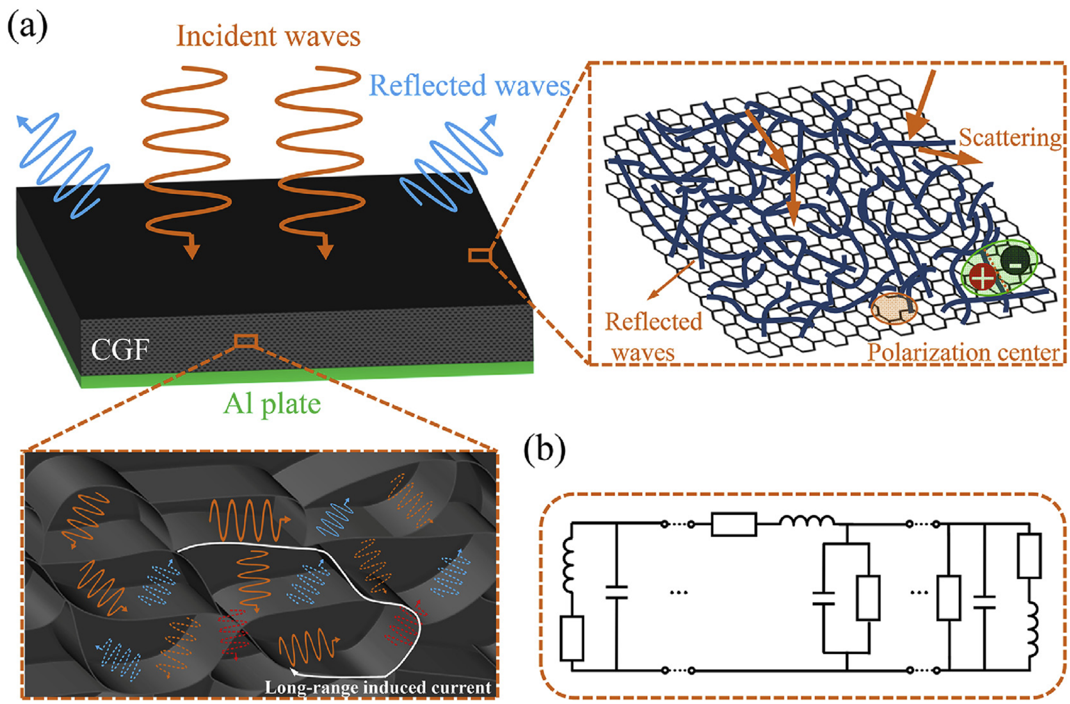

Fig. 7. (a) Schematic representation of electromagnetic wave attenuation mechanism of CGFs. (b) Schematic illustration of the formation of numerous resistance-inductance-capacitance coupled circuits in 3D CGF for responding to incident electromagnetic wave. (A colour version of this figure can be viewed online.)

new MWCNT network is formed within CGFs (Fig. 3i–k). This MWCNT network weakens the stacking of graphene sheets, strengthens the conductive network, thus enhance polarization loss and conduction loss. The integrated MWCNT/graphene network form a giant 3D cross-linked and intricate conductive network. This creates extremely long and complex transmission channel for the incoming electromagnetic wave (Fig. 7a) and then intensely responses to the incident electromagnetic wave as massive resistance–inductance–capacitance coupled circuits and time-varying electromagnetic fields-induced currents among the framework of CGFs (Fig. 7b) [22,54–57]. This would induce currents among the resistive 3D MWCNT/graphene network under alternating electromagnetic field contributes to ohmic losses [58], resulting in sufficient attenuation for the energy of the propagated electromagnetic wave.

4. Conclusion

In summary, we have successfully fabricated a series of ultralight CGFs through facile solvothermal process. Through varying initial MWCNT loading and latter annealing temperature, the complex permittivity, electrical conductivity and microstructure of CGFs can be regulated conveniently. The optimized CGFs (CG2F-200, CG3F-200 and CG7F-400) exhibit ultra-broad qualified bandwidth (covering C band, X band, Ku band, and most of S band) and prominent *AAI* (over 20 dB) in both C and X bands. Particularly, an entire qualified bandwidth of 16 GHz (2–18 GHz) and minimum RL value of −39.5 dB, together with incredible *AAI* of 19.1 dB in 2–18 GHz and 22.7 dB in 4–12 GHz are achieved by the ultralight CG7F-400. This is superior to available MAMs in open literature. It is believed that the well balance between impedance matching and electromagnetic wave attenuation as well as the distinctive 3D interconnected and intricate loss network with the synergistic effect of MWCNT and graphene endow the CGFs with impressive MA performance. We believe that the ultralight MA CGF will prove its value in military equipment and privacy protection.

Acknowledgements

The authors gratefully acknowledge the financial support from MOST (2016YFA0200200), NSFC (21374050, 51373078, and 51422304), and NSF of Tianjin City (15JCYBJC17700).

Appendix A. Supplementary data

Supplementary data related to this article can be found at https://doi.org/10.1016/j.carbon.2017.09.007.

References

[1] H. Xu, X. Yin, M. Zhu, M. Han, Z. Hou, X. Li, et al., Carbon hollow microspheres with a designable mesoporous shell for high-performance electromagnetic wave absorption, ACS Appl. Mater. Interfaces 9 (2017) 6332–6341.
[2] Q. Liu, Q. Cao, H. Bi, C. Liang, K. Yuan, W. She, et al., CoNi@SiO2@TiO2 and CoNi@Air@TiO2 microspheres with strong wideband microwave absorption, Adv. Mater. 28 (2016) 486–490.
[3] H. Yang, M. Cao, Y. Li, H. Shi, Z. Hou, X. Fang, et al., Enhanced dielectric properties and excellent microwave absorption of SiC powders driven with NiO nanorings, Adv. Opt. Mater. 2 (2014) 214–219.
[4] Z. Fan, G. Luo, Z. Zhang, L. Zhou, F. Wei, Electromagnetic and microwave absorbing properties of multi-walled carbon nanotubes/polymer composites, Mater. Sci. Eng. B 132 (2006) 85–89.
[5] Y. Zhang, Y. Huang, H. Chen, Z. Huang, Y. Yang, P. Xiao, et al., Composition and structure control of ultralight graphene foam for high-performance microwave absorption, Carbon 105 (2016) 438–447.
[6] Q. Zeng, X.-H. Xiong, P. Chen, Q. Yu, Q. Wang, R.-C. Wang, et al., Air@rGO-sicFe(3)O(4) microspheres with spongy shells: self-assembly and microwave absorption performance, J. Mater. Chem. C 4 (2016) 10518–10528.
[7] Y. Qing, W. Zhou, F. Luo, D. Zhu, Epoxy-silicone filled with multi-walled carbon nanotubes and carbonyl iron particles as a microwave absorber, Carbon 48 (2010) 4074–4080.
[8] W. You, H. Bi, W. She, Y. Zhang, R. Che, Dipolar-distribution cavity gamma-Fe2O3@C@alpha-MnO2 nanospindle with broadened microwave absorption bandwidth by chemically etching, Small (2017), http://dx.doi.org/10.1002/smll.201602779.
[9] Y. Chen, X. Liu, X. Mao, Q. Zhuang, Z. Xie, Z. Han, [gamma]-Fe2O3-MWNT/poly(p-phenylenebenzobisoxazole) composites with excellent microwave

absorption performance and thermal stability, Nanoscale 6 (2014) 6440–6447.
[10] R. Yang, B. Wang, J. Xiang, C. Mu, C. Zhang, F. Wen, et al., Fabrication of NiCo2-anchored graphene nanosheets by liquid-phase exfoliation for excellent microwave absorbers, ACS Appl. Mater. Interfaces 9 (2017) 12673–12679.
[11] G. Sun, B. Dong, M. Cao, B. Wei, C. Hu, Hierarchical dendrite-like magnetic materials of Fe3O4, gamma-Fe2O3, and Fe with high performance of microwave absorption, Chem. Mater. 23 (2011) 1587–1593.
[12] H. Sun, R. Che, X. You, Y. Jiang, Z. Yang, J. Deng, et al., Cross-stacking aligned carbon-nanotube films to tune microwave absorption frequencies and increase absorption intensities, Adv. Mater 26 (2014) 8120–8125.
[13] Z-z Wang, P-h Lin, W-c Huang, S-k Pan, Y. Liu, L. Wang, Effect of Ni content on microwave absorbing properties of MnAl powder, J. Magn. Magn. Mater. 413 (2016) 9–13.
[14] H.J. Yang, W.Q. Cao, D.Q. Zhang, T.J. Su, H.L. Shi, W.Z. Wang, et al., NiO hierarchical nanorings on SiC: enhancing relaxation to tune microwave absorption at elevated temperature, ACS Appl. Mater. Interfaces 7 (2015) 7073–7077.
[15] H. Zhou, J. Wang, J. Zhuang, Q. Liu, A covalent route for efficient surface modification of ordered mesoporous carbon as high performance microwave absorbers, Nanoscale 5 (2013) 12502–12511.
[16] Z. Chen, C. Xu, C. Ma, W. Ren, H.M. Cheng, Lightweight and flexible graphene foam composites for high-performance electromagnetic interference shielding, Adv. Mater. 25 (2013) 1296–1300.
[17] X.H. Li, X. Li, K.N. Liao, P. Min, T. Liu, A. Dasari, et al., Thermally annealed anisotropic graphene aerogels and their electrically conductive epoxy composites with excellent electromagnetic interference shielding efficiencies, ACS Appl. Mater. Interfaces 8 (2016) 33230–33239.
[18] B. Shen, Y. Li, D. Yi, W. Zhai, X. Wei, W. Zheng, Microcellular graphene foam for improved broadband electromagnetic interference shielding, Carbon 102 (2016) 154–160.
[19] W. Lv, C. Zhang, Z. Li, Q.-H. Yang, Self-assembled 3D graphene monolith from solution, J. Phys. Chem. Lett. 6 (2015) 658–668.
[20] C. Li, G. Shi, Three-dimensional graphene architectures, Nanoscale 4 (2012) 5549–5563.
[21] P. Zhang, J. Li, L. Lv, Y. Zhao, L. Qu, Vertically aligned graphene sheets membrane for highly efficient solar thermal generation of clean water, ACS Nano 11 (2017) 5087–5093.
[22] Y. Zhang, Y. Huang, T. Zhang, H. Chang, P. Xiao, H. Chen, et al., Broadband and tunable high-performance microwave absorption of an ultralight and highly compressible graphene foam, Adv. Mater. 27 (2015) 2049–2053.
[23] L. Kong, X. Yin, X. Yuan, Y. Zhang, X. Liu, L. Cheng, et al., Electromagnetic wave absorption properties of graphene modified with carbon nanotube/poly(dimethyl siloxane) composites, Carbon 73 (2014) 185–193.
[24] W.-L. Song, X.-T. Guan, L.-Z. Fan, Y.-B. Zhao, W.-Q. Cao, C.-Y. Wang, et al., Strong and thermostable polymeric graphene/silica textile for lightweight practical microwave absorption composites, Carbon 100 (2016) 109–117.
[25] Y. Wang, W. Zhang, X. Wu, C. Luo, T. Liang, G. Yan, Metal-organic framework nanoparticles decorated with graphene: a high-performance electromagnetic wave absorber, J. Magn. Magn. Mater. 416 (2016) 226–230.
[26] H. Sun, Z. Xu, C. Gao, Multifunctional, ultra-flyweight, synergistically assembled carbon aerogels, Adv. Mater. 25 (2013) 2554–2560.
[27] L. Peng, Y. Feng, P. Lv, D. Lei, Y. Shen, Y. Li, et al., Transparent, conductive, and flexible multiwalled carbon nanotube/graphene hybrid electrodes with two three-dimensional microstructures, J. Phys. Chem. C 116 (2012) 4970–4978.
[28] M. Kotal, A.K. Bhowmick, Multifunctional hybrid materials based on carbon nanotube chemically bonded to reduced graphene oxide, J. Phys. Chem. C 117 (2013) 25865–25875.
[29] V. Sridhar, I. Lee, H.-H. Chun, H. Park, Microwave synthesis of nitrogen-doped carbon nanotubes anchored on graphene substrates, Carbon 87 (2015) 186–192.
[30] R.C. Che, L.M. Peng, X.F. Duan, Q. Chen, X.L. Liang, Microwave absorption enhancement and complex permittivity and permeability of Fe encapsulated within carbon nanotubes, Adv. Mater. 16 (2004) 401–405.
[31] B. Wen, M.-S. Cao, Z.-L. Hou, W.-L. Song, L. Zhang, M.-M. Lu, et al., Temperature dependent microwave attenuation behavior for carbon-nanotube/silica composites, Carbon 65 (2013) 124–139.
[32] R.H. Baughman, A.A. Zakhidov, W.A. de Heer, Carbon nanotubes - the route toward applications, Science 297 (2002) 787–792.
[33] H. Nikmanesh, M. Moradi, G.H. Bordbar, R.S. Alam, Synthesis of multi-walled carbon nanotube/doped barium hexaferrite nanocomposites: an investigation of structural, magnetic and microwave absorption properties, Ceram. Int. 42 (2016) 14342–14349.
[34] J. Li, L. Qi, H. Li, Facile strategy to prepare light-weight PVA membrane based on schiff base derivatives and MWCNTs for electromagnetic wave absorption, J. Phys. Chem. C 120 (2016) 22865–22872.
[35] Z. Liu, G. Bai, Y. Huang, F. Li, Y. Ma, T. Guo, et al., Microwave absorption of single-walled carbon nanotubes/soluble cross-linked polyurethane composites, J. Phys. Chem. C 111 (2007) 13696–13700.
[36] Z. Zeng, H. Jin, M. Chen, W. Li, L. Zhou, Z. Zhang, Lightweight and anisotropic porous MWCNT/WPU composites for ultrahigh performance electromagnetic interference shielding, Adv. Funct. Mater. 26 (2016) 303–310.
[37] Y. Chen, H.-B. Zhang, Y. Yang, M. Wang, A. Cao, Z.-Z. Yu, High-performance epoxy nanocomposites reinforced with three-dimensional carbon nanotube sponge for electromagnetic interference shielding, Adv. Funct. Mater. 26 (2016) 447–455.
[38] Y. Wu, N. Yi, L. Huang, T. Zhang, S. Fang, H. Chang, et al., Three-dimensionally bonded spongy graphene material with super compressive elasticity and near-zero Poisson's ratio, Nat. Commun. 6 (2015) 6141.
[39] K.A. Wepasnick, B.A. Smith, K.E. Schrote, H.K. Wilson, S.R. Diegelmann, D.H. Fairbrother, Surface and structural characterization of multi-walled carbon nanotubes following different oxidative treatments, Carbon 49 (2011) 24–36.
[40] C.-Y. Su, Y. Xu, W. Zhang, J. Zhao, A. Liu, X. Tang, et al., Highly efficient restoration of graphitic structure in graphene oxide using alcohol vapors, ACS Nano 4 (2010) 5285–5292.
[41] Z. Yan, Z.W. Peng, G. Casillas, J. Lin, C.S. Xiang, H.Q. Zhou, et al., Rebar graphene, ACS Nano 8 (2014) 5061–5068.
[42] Y. Huang, H. Zhang, G. Zeng, Z. Li, D. Zhang, H. Zhu, et al., The microwave absorption properties of carbon-encapsulated nickel nanoparticles/silicone resin flexible absorbing material, J. Alloys Compd. 682 (2016) 138–143.
[43] B. Zhao, X. Guo, W. Zhao, J. Deng, G. Shao, B. Fan, et al., Yolk-shell Ni@SnO2 composites with a designable interspace to improve the electromagnetic wave absorption properties, ACS Appl. Mater. Interfaces 8 (2016) 28917–28925.
[44] J.A. Bruder, IEEE radar standards and the radar systems panel, IEEE Aerosp. Electron Syst. Mag. 28 (2013) 19–22.
[45] Z. Fang, X. Cao, C. Li, H. Zhang, J. Zhang, H. Zhang, Investigation of carbon foams as microwave absorber: numerical prediction and experimental validation, Carbon 44 (2006) 3368–3370.
[46] Z. Fang, C. Li, H. Sun, H. Zhang, J. Zhang, The electromagnetic characteristics of carbon foams, Carbon 45 (2007) 2873–2879.
[47] T.C. Zou, N.Q. Zhao, C.S. Shi, J.J. Li, Microwave absorbing properties of activated carbon fibre polymer composites, Bull. Mater. Sci. 34 (2011) 75–79.
[48] J. Yang, Z.M. Shen, Z.B. Hao, Microwave characteristics of sandwich composites with mesophase pitch carbon foams as core, Carbon 42 (2004) 1882–1885.
[49] W. Liu, H. Li, Q. Zeng, H. Duan, Y. Guo, X. Liu, et al., Fabrication of ultralight three-dimensional graphene networks with strong electromagnetic wave absorption properties, J. Mater. Chem. A 3 (2015) 3739–3747.
[50] A.P. Singh, M. Mishra, P. Sambyal, B.K. Gupta, B.P. Singh, A. Chandra, et al., Encapsulation of [gamma]-Fe2O3 decorated reduced graphene oxide in polyaniline core-shell tubes as an exceptional tracker for electromagnetic environmental pollution, J. Mater. Chem. A 2 (2014) 3581–3593.
[51] Y. Ding, Z. Zhang, B. Luo, Q. Liao, S. Liu, Y. Liu, et al., Investigation on the broadband electromagnetic wave absorption properties and mechanism of Co3O4-nanosheets/reduced-graphene-oxide composite, Nano Res. 10 (2017) 980–990.
[52] Y.-H. Chen, Z.-H. Huang, M.-M. Lu, W.-Q. Cao, J. Yuan, D.-Q. Zhang, et al., 3D Fe3O4 nanocrystals decorating carbon nanotubes to tune electromagnetic properties and enhance microwave absorption capacity, J. Mater. Chem. A 3 (2015) 12621–12625.
[53] J. Xi, E. Zhou, Y. Liu, W. Gao, J. Ying, Z. Chen, et al., Wood-based straightway channel structure for high performance microwave absorption, Carbon 124 (2017) 492–498, http://dx.doi.org/10.1016/j.carbon.2017.07.088.
[54] F. Shahzad, M. Alhabeb, C.B. Hatter, B. Anasori, S.M. Hong, C.M. Koo, et al., Electromagnetic interference shielding with 2D transition metal carbides (MXenes), Science 353 (2016) 1137–1140.
[55] D.-X. Yan, H. Pang, B. Li, R. Vajtai, L. Xu, P.-G. Ren, et al., Structured reduced graphene oxide/polymer composites for ultra-efficient electromagnetic interference shielding, Adv. Funct. Mater. 25 (2015) 559–566.
[56] N. Yousefi, X. Sun, X. Lin, X. Shen, J. Jia, B. Zhang, et al., Highly aligned graphene/polymer nanocomposites with excellent dielectric properties for high-performance electromagnetic interference shielding, Adv. Mater. 26 (2014) 5480–5487.
[57] H. Zhang, J. Zhang, H. Zhang, Computation of radar absorbing silicon carbide foams and their silica matrix composites, Comput. Mater. Sci. 38 (2007) 857–864.
[58] D. Micheli, R.B. Morles, M. Marchetti, F. Moglie, V.M. Primiani, Broadband electromagnetic characterization of carbon foam to metal contact, Carbon 68 (2014) 149–158.